RAPID COMMUNICATIONS IN MASS SPECTROMETRY, VOL. **11**, 1467–1477 (1997)

Simulation of External Ion Injection, Cooling and Extraction Processes with SIMION 6.0 for the Ion Trap/Reflectron Time-of-flight Mass Spectrometer

Ling He and David M. Lubman*

Department of Chemistry, The University of Michigan, Ann Arbor, MI 48109-1055, USA

SPONSOR REFEREE: C. Lifshitz, Department of Physical Chemistry, The Hebrew University of Jerusalem, Givat Ram, Jerusalem 91904, Israel

In this work we have developed a PC-based simulation to study ion injection, cooling and extraction processes for multiple ions in an ion trap/reflectron time-of-flight (IT/reTOF) system. This simulation is based upon SIMION 6.0 with user written programs in which a 3D collision model is used to describe ion – buffer gas molecule interactions. The results of various simulations describing the relation between the trapping efficiency for external injection of ions into the trap and the RF phase, and the effects of initial kinetic energy and ramp-up rate on dynamic trapping of externally produced ions are discussed. Further, single-pulsing and bipolar-pulsing schemes for ejecting ions from the trap are examined. The simulations show that bipolar pulsing can markedly improve the resolution. In the bipolar ejection mode the relation between resolution and the extraction voltages and RF ramp-off rate are studied.

Received 18 July 1997; Accepted 22 July 1997
Rapid. Commun. Mass Spectrom. **11**, 1467–1477 (1997)
No. of Figures: 14 No. of Tables: 0 No. of Refs: 28

The quadrupole ion trap (QUISTOR) has become a widely used mass spectrometer based upon the development of the mass selective ejection[1] mode in which ions are ejected from the trap for detection as the RF voltage is scanned. In more recent work though, a hybrid ion trap/reflectron time-of-flight (IT/reTOF) device has been developed in which the ion trap serves as a front end storage device prior to analysis by a reTOF device.[2] In this hybrid device the ions are stored in the trap for a certain period of time and then simultaneously ejected by a DC pulse for detection in a reTOF. This configuration has several advantages for detection of on-line separations including speed of detection due to the non-scanning nature of the device and sensitivity due to the high duty cycle and ion storage properties of the trap. In recent work the IT/reTOFMS has been used with electrospray ionization for on-line detection of fast capillary electrophoresis (CE) and capillary electrochromatography (CEC) separations for solving biological problems based upon the speed and sensitivity of the device.[3,4] The tandem mass spectrometry (MS/MS) capabilities of the trap make it a powerful method of obtaining structural analysis in these on-line separations.[5–7] In addition, the IT/reTOF has been interfaced to pulsed ionization sources such as matrix-assisted laser desorption/ionization (MALDI) for studying biological samples.[8,9]

To improve the sensitivity and resolution of the IT/reTOF system, it is necessary to understand ion injection and extraction processes and the related control parameters. Simulations of single ion motion inside the ion trap[10–13] can describe the resonant excitation and ejection behaviors. Cooks and his colleagues have developed a PC-based software package to simulate multiple ion trajectories inside the ion trap[14,15] where factors such as ion–ion and ion–buffer gas interactions are considered in their program to explore buffer gas effects, resonant excitation processes and methods for improving external ion injection trapping efficiency.

In this article SIMION 6.0 is the main program used to simulate multiple ion behavior in the IT/reTOF mass spectrometer. The potential array in the ion trap and acceleration region is calculated using the SIMION program. User-written programs are implemented in the SIMION main program to change the RF potential applied to the ring electrode in the ion injection and trapping processes and to apply DC pulse(s) to the end cap(s) to eject ions from the ion trap for TOF mass detection. One important feature of the current program is that we have implemented a 3D orthogonal hard-sphere collision model to simulate the collisional kinetic energy damping effects of buffer gases. The mean free path is dynamically adjusted according to the ions' averaged velocity. This model is more appropriate for describing the trajectories of ions after random collisions with buffer gas molecules as opposed to head-on collisions, where momentum exchange only causes energy losses and scattering effects are ignored.

The sensitivity of an IT/reTOF system is dependent on the trapping efficiency. Ions can enter the ion trap through the center of the entrance end cap (axial injection), the midpoint of the ring electrode (radial injection) or the gaps between the end caps and the ring electrode (asymptotic injection). In asymptotic injection the high electric field between the ring electrode

*Correspondence to: D. M. Lubman, Department of Chemistry, The University of Michigan, Ann Arbor, MI 48109-1055, USA
Contract grant sponsor: National Institutes of Health; Contract grant number: IR01GM49500
Contract grant sponsor: National Center for Human Genome Research; Contract grant number: IR01HG0068503
Contract grant sponsor: National Science Foundation; Contract grant number: BIR9513878

CCC 0951–4198/97/131467–11 $17.50

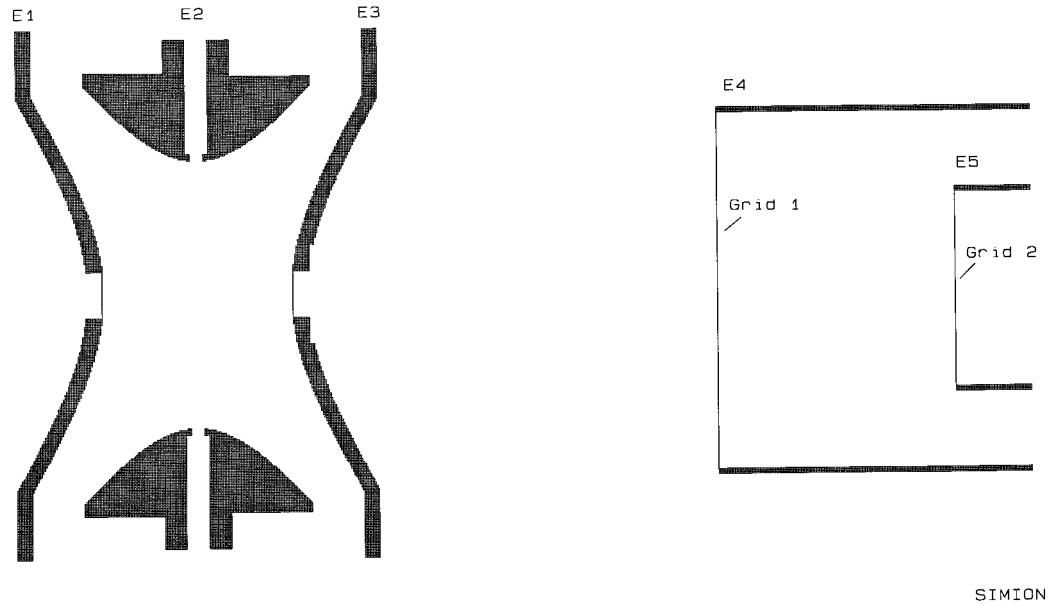

Figure 1. The quadrupole ion trap and the acceleration region.

and the end cap quickly deflects the ions to an electrode so that this is not an efficient method. For ions generated in the pulsed mode (MALDI, fast-atom bombardment), the RF potential applied to the ring electrode could be gated in synchronization with the short ion pulse and theoretically high trapping efficiency could be achieved[16,17] so that ions can enter the ion trap either radially or axially. This method has not been realized due to the difficulty involved in turning on the RF voltage with high accuracy phase synchronization of the RF frequency. Another more practical approach, called dynamic trapping,[18–21] involves turning off or lowering the RF potential when ions enter the ion trap axially and then ramping it up gradually as the ions move towards the center of the ion trap. An investigation of ion injection schemes using numerical methods have shown that axial injection is advantageous over the radial and asymptotic injections.[22] In this simulation study, we have investigated the relationship between the trapping efficiency and the parameters such as the initial kinetic energy of the ions, RF phase, RF ramp-up rate, etc.

The resolution of the IT/reTOF system is also determined by the initial conditions for accelerating the ions into the field free region. To avoid the influence of the phase of the RF voltage on the extraction process the RF voltage is rapidly shut down before the extraction process begins. The factors which influence the resolution include the initial space distribution and kinetic energy distribution of the ions, m/z, pulsing voltage, single pulsing or bipolar pulsing and RF shutdown speed. Because of the collisional cooling effect, the contribution from the initial kinetic energy distribution is negligible and other factors described herein will be studied.

METHOD

The software packages used in this work are SIMION 6.0 (Princeton Electronic Systems, Princeton, NJ, USA) and MathCad 6.0 Student Edition (Mathsoft). The 3D quadrupole ion trap and the ion acceleration region are modeled as shown in Fig. 1. The physical dimensions of the ion trap are: z_0 = 0.707 cm, r_0 = 1.0 cm, where z_0 represents half of the shortest distance between the two end caps and r_0 represents the radius of the ring electrode. Five electrodes are included in the simulation: E1 — entrance end cap, E2 — ring electrode, E3 — exit electrode, E4 — the acceleration grid, E5 — the first cylindrical lens of the einzel lens. The voltages applied to E4 and E5 are –2000 V. The curve of the internal surface of the quadrupole ion trap is created using a geometry file, a feature provided by SIMION 6.0 which can be used to mathematically define the hyperbolic internal surface shape. The r_0 and z_0 parameters defined in the geometry file could be varied to simulate any general form of quadrupole ion trap.[23] In the simulation presented in this work, 1 grid unit in the 2D matrix corresponds to 0.125 mm in the real ion trap. The high precision used here ensures very accurate calculation of ion movement inside the ion trap. The rapid oscillating electric field inside the ion trap and sharp potential gradient between E3 and E4 also requires a high density matrix to calculate each ion's position and kinetic energy in the acceleration process, i.e. the process which ultimately determines resolution. The potential array updating speed is dynamically adjusted by SIMION and the time step for upgrading is usually much smaller than the maximum time step (0.05 μs) set by the user program. Although the ion–ion repulsion effects can be approximated in the SIMION program, it is not considered since only a limited number of ions ($\leq$ 200 ions) are in the trap. The resulting simulation can provide systematic results concerning the trapping and extraction processes.

RF potential

The RF potential on the ring electrode is controlled by user-written programs. The function which describes the potential applied to the ring electrode of the quadrupole ion trap is: $V_{RF} = U_0 + V_0\cos(2\pi\Omega t + \beta_0)$, where U_0 is the DC voltage (set to be 0 V in current program), V_0 is the maximum amplitude of the RF

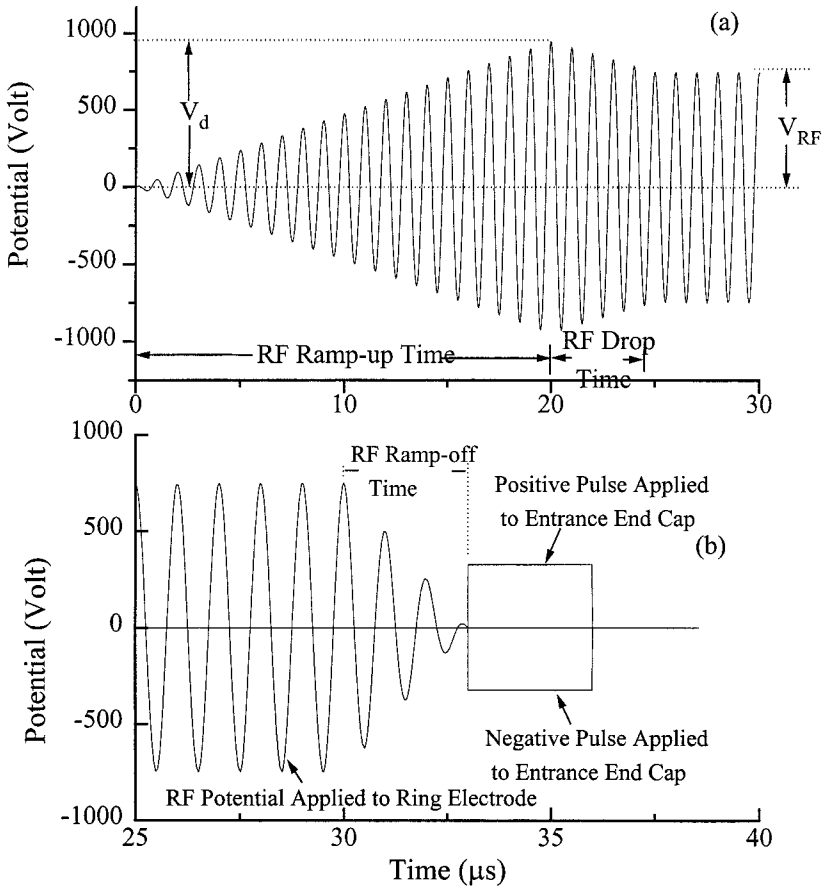

Figure 2. (a) The initial RF potential in dynamic trapping mode, (b) the RF and extraction voltages during the extraction.

potential, Ω is the RF frequency (set to be 1.0 MHz), β_0 is the initial RF phase (set to be 0 in current program) and t is the ion flight time. The amplitude of the RF potential is dynamically tuned by the user program in simulating the dynamic trapping and ion extraction processes. The initial RF potentials in normal and dynamic trapping processes are shown in Fig. 2(a) and (b). In Fig. 2 (a), the RF potential first ramps up from an initial RF potential (V_{init}, set to 0 V) to a higher value (V_d) and drops back to the normal RF amplitude. The change of the RF amplitude is in a linear relationship with time elapsed in the rise and drop interval. The initial RF potential, ramp-up time, drop time and V_d can all be determined by the user beforehand. In Fig. 2 (b) is also shown the RF potential damping process at the end of the trapping. DC pulses are applied to E1 and E3 at the end of the RF shut-down. The trapping time, RF ramp-off time, pulse potential, pulse width, and the pulse starting time can all be set by the user program to investigate ion extraction.

Ion generation

In these simulations 200 ions are used to obtain statistical results with the user program to simulate the ion injection process and 50 ions are used in simulating the extraction process. All the ions are assumed to be positively, singly charged ions. The MathCad program is used to generate random numbers of Gaussian distribution. For simulating ion injection, all the ions start at the same z (axial) position (the position of the grid on the apex of the entrance end cap) while their initial x and y positions are generated with a Gaussian distribution. The standard deviation (σ) for initial x and y positions is 1.0 mm. The ion injection angle is defined by two components, azimuth and elevation angles. Each component has its own Gaussian distribution in the –5 ° to 5 ° range. The kinetic energy of all the ions in one packet are identical. To observe the effects of initial kinetic energy in the ion injection process different ion packets are used. For the extraction process simulation, the ions are generated around the center of the ion trap. For their initial x, y, z positions, each has it own Gaussian distribution with a standard deviation of 0.41 mm. The initial kinetic energy assigned to these ions is 0.1 eV. The ions will oscillate inside the ion trap for 30 μs before the extraction pulse is applied, thus the initial conditions for extraction are randomized by the program itself so that it results in a relatively realistic representation of ion motion in the trap.

Buffer gas effect

One important feature of our user program is that we have for the first time implemented a 3D hard sphere collision model for simulating the ion–buffer gas interactions. The ion–neutral interactions occur randomly in time, space and velocity. Since the buffer gas molecules may move towards the ion or leave the ion along the direction of the relative velocity before they collide (Fig. 3(a)), statistically the ion and the buffer gas approach the collision point at a 90 ° angle relative to each other. Given a 3D vector of an ion's velocity (V_i),

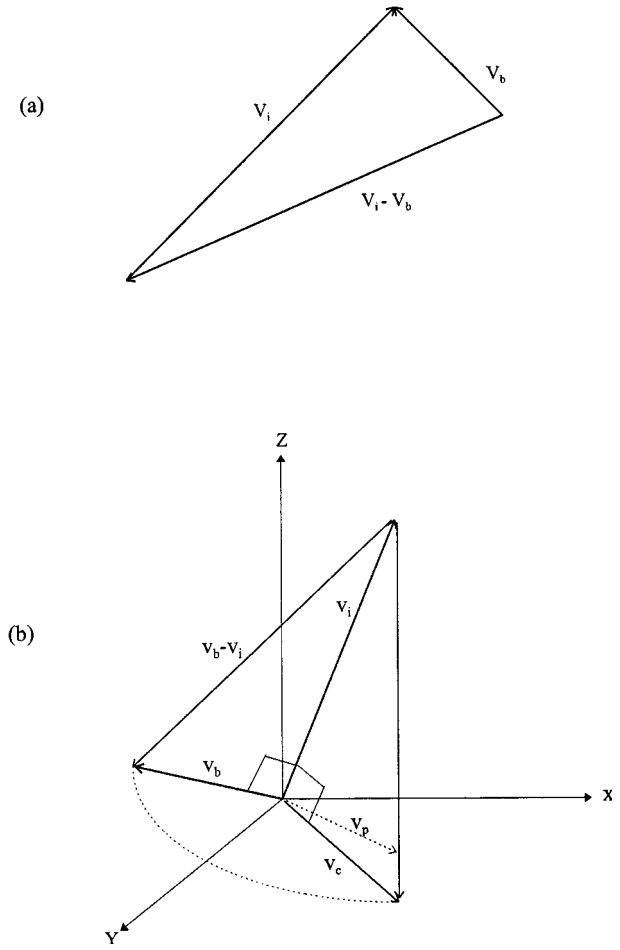

Figure 3. (a) The orthogonal collision model. V_i is the velocity vector of the ion and V_b is the velocity vector of the buffer gas. (b) The random velocity vector generation process of buffer gas molecules. The ion velocity vector V_i is first projected to the x–y plane and a vector V_p is obtained. V_p and V_i are used to calculate V_c, a vector which is orthogonal to V_i but is on the V_i–V_p plane. V_c is then rotated for a random angle on the plane which is vertical to V_i and a vector V_b is obtained. V_b is the actual velocity vector of the buffer gas molecule for calculating the collision with an ion.

we can generate a 3D buffer gas velocity vector (V_b) by rotating a vector (V_c) which is vertical to V_i for a random degree (0 ° ~ 360 °) V_i and V_b are then used to calculate the new velocity vector for the ion after the collision (Fig. 3(b)).

The collision frequency for an ion is calculated using the following function

$$q = N\sigma(V_{ion}^2 + V_{buf}^2)^{1/2} \quad (1)$$

where V_{ion} and V_{buf} are the average velocities of the ion and buffer gas molecule, N is the number of buffer molecules in one unit volume calculated using the ideal gas law, σ is the collision cross section and $(V_{ion}^2 + V_{buf}^2)^{1/2}$ is the relative speed between the ion and the buffer gas. In this article the pressure inside the ion trap is assumed to be 4 mTorr, the diameter of the ion is assumed to be 15 Å, the diameter and molecular weight of the buffer gas molecule is assumed to be 2 Å and 4 amu. The mean free path of the ion under a certain collision frequency is

$$\lambda_m = V_{ion}/q \quad (2)$$

Equations (1) and (2) are standard equations which are used to calculate q and λ_m for collisions between two different gas phase molecules with no electric field and V_{ion} does not change between two collisions. Since the velocity of an ion changes when the ion oscillates inside the ion trap due to the RF driving potential, at each time step we calculate V_{ion} by dividing the path the ion has passed (L_p) since the last collision by the time of this period (T_p). V_{ion} is then an averaged speed and is the value which is used to calculate the λ_m. If L_p is larger than the λ_m, then there is a collision. If not, the current time step (δt) is added to T_p and $\delta t \times V_i$ is added to L_p. This process iterates until L_p is larger than λ_m and consequently a collision occurs. T_p and L_p are then set to 0 and the above steps are repeated for determining the occurrence of the next collision event. In the current program, the calculated mean free path is multiplied by a factor (random number in the range 0.7 ~ 1.3, in our case) before it is compared with L_p. This factor is used to represent the random-in-time property of the collision process since the collision may take place before or after the calculated mean free path is reached. If the factor is fixed at 1, the randomness for the time intervals of the collisions is minimized. The reason for using the averaged velocity and integrated path to decide whether a collision will occur involves using a small number of ions (200) to represent the behaviour of a much larger number of ions in the ion trap ($\sim 10^5$–10^6 ions). Since T_p and L_p record the information of ion movement starting from the end of the previous collision, statistically this method is more reliable than using the current ion velocity to predict the possibilities of ion–neutral collisions.

Compared to the 2D head-on hard sphere collision model, a major advantage of the 3D collision model is that it considers the random nature of the buffer gas velocities. For smaller ions, collisions with neutral buffer gas molecules may scatter the ions instead of just removing kinetic energy. For ions moving around the center of the ion trap the scattering effect does not significantly influence the trapping efficiency. However, for ions moving close to the boundary of the ion trap the scattering effect is an important factor which causes ion loss. The difference between the 2D and 3D collision models is shown in Fig. 4. Assuming the electric potential is 0 and only collisions with neutral gas molecules cause the loss of kinetic energy, the velocity of ions vs. number of collisions in both collision models for a molecule of 200 amu and 24 eV initial kinetic energy is shown in Fig. 4(a) and (b). It is observed that in the orthogonal collision model the energy damping process is slower and smoother since each orthogonal collision removes less kinetic energy from the ion.

RESULTS AND DISCUSSION

Energy damping in external ion injection

To efficiently trap ions which enter the ion trap through the entrance end cap, it is necessary to remove the kinetic energy with a buffer gas. The motions of ions inside the ion trap are strongly dependent on the initial conditions such as RF phase upon injection and the initial kinetic energy of the ions. Fisher[25] showed that without the damping effect accompanying the presence

of a buffer gas, an infinite trapping of ions injected at a constant RF potential is impossible. As described by the pseudo-potential theory, without a buffer gas the ions will continue to oscillate inside the ion trap and the amplitude will not be reduced. The quadrupole field inside the ion trap is 'imperfect' because of holes on the electrodes, finite dimensions of the electrodes and imperfections in machining. Externally injected ions which oscillate back to the boundary of the internal surface of the ion trap will be disturbed by the electric fields created by those factors and eventually escape from the ion trap. The momentum exchange when the ions collide with buffer gas molecules provides a means for the ions to lose their kinetic energy and oscillate only at the bottom of the potential well — which is at the center of the ion trap. The energy damping process in the normal trapping mode for 10 ions is shown in Fig. 5(a) and (b). The initial kinetic energy is 25 eV and 15 eV, respectively. The initial RF phases are 200 °, a phase angle which falls in the optimal ion injection phase range for those ions (simulation results shown later). The kinetic energy is averaged for each RF cycle (1 μs step). It can be seen that the energy damping processes are very similar for ions of two different initial kinetic energies if they enter the ion trap at the same initial RF phase. The ions are accelerated and decelerated repeatedly as they oscillate inside the ion trap. In both cases it requires about 100 μs to remove ~ 97% of the initial kinetic energy. This energy damping rate is also mass dependent, where the energy drop for larger ions will be slower because each collision with the buffer gas removes less kinetic energy than for smaller ions.

In the dynamic trapping mode, the RF is 0 V when the ions enter the ion trap and it is then ramped up as the ions enter the ion trap. It is necessary to ramp up the RF sufficiently fast so that the potential well depth is of sufficient magnitude before the ions reach the other electrode. The dynamic trapping scheme modeled here is called 'matched dynamic trapping',[19–21] where the RF potential is ramped to a higher value than the final trapping potential to create a deeper potential well in the ion injection and trapping process. The energy damping process is shown in Fig. 5(c) and (d). The initial kinetic energy is 2.5 eV and 5 eV (significant ion loss occurs at higher initial kinetic energy under the current conditions, which will be discussed later) and 10

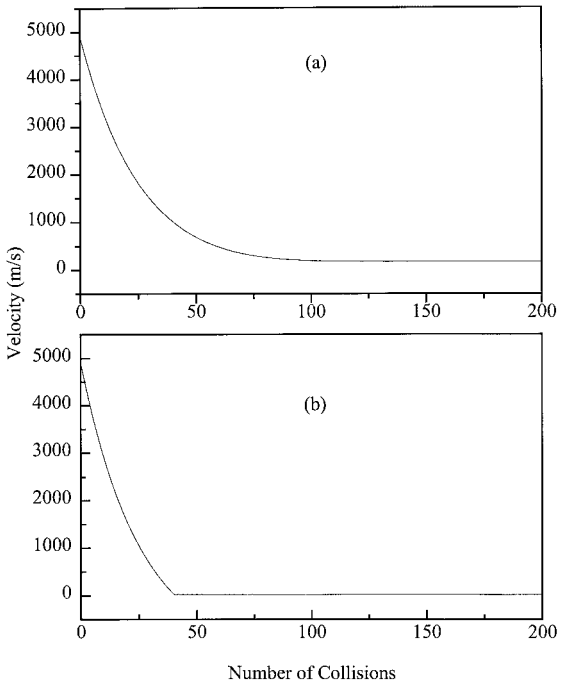

Figure 4. Velocity of ions vs. collision times in (a) 3D orthogonal collision modeling, (b) 2D head-on collision modeling. Molecular weight of the buffer gas molecule is 4 amu and molecular diameter is 2 Å. Molecular weight of the ion is 200 amu, molecular diameter is 15 Å.

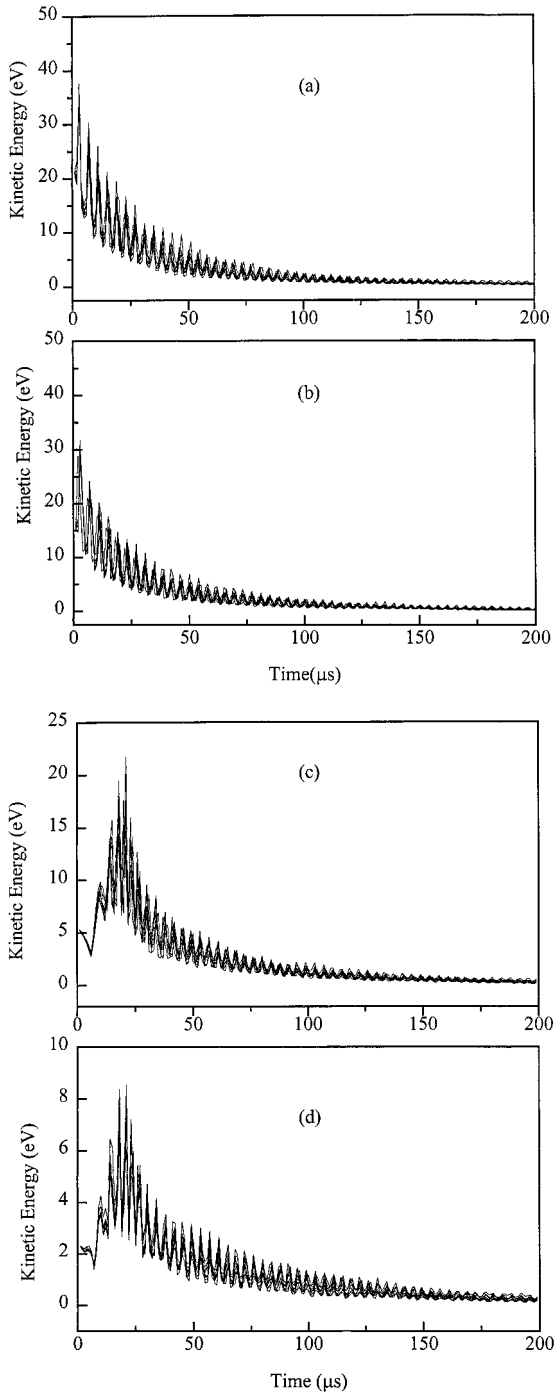

Figure 5. The energy damping in the external ion injection process. External ion injection in normal trapping mode with (a) 25 eV initial kinetic energy, 200 ° initial RF phase angle, (b) 15 eV initial kinetic energy, 200 ° initial RF phase angle. External ion injection in dynamic trapping mode with (c) 5 eV initial kinetic energy, (d) 2.5 eV initial kinetic energy. The RF ramp-up time is 20 μs and the drop time is 10 μs. V_d = 950 $V_{0\text{-}p}$, V_{RF} = 750 $V_{0\text{-}p}$.

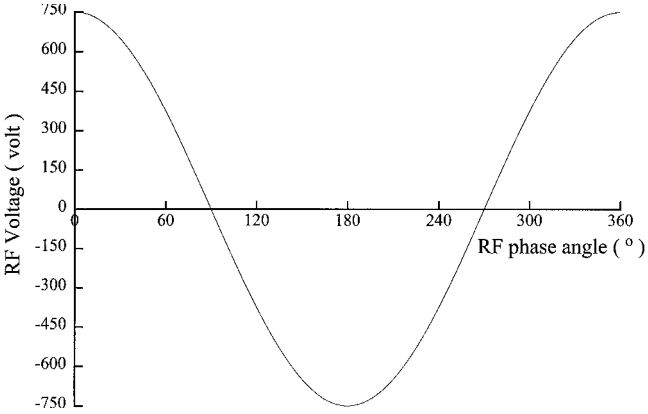

Figure 6. The relation between the RF potential and the RF phase angle.

ions are used in each case. The RF potential ramps up from 0 V to 950 $V_{0\text{-}p}$ in 20 μs and drops back to 750 $V_{p\text{-}p}$ (peak to peak) in 10 μs. It is interesting to observe that even though the initial kinetic energy of the ions are relatively low, they continue to gain kinetic energy as the RF increases and the maximum kinetic energy is reached at around 20 μs, when the trapping potential well for the ions is deepest. The kinetic energy drops after 20 μs and the energy damping pattern is similar to the normal trapping mode.

Trapping efficiency in external ion injection for positive ions

In the normal trapping mode, ions enter the ion trap at different RF phases and consequently experience different trajectories. The relationship between the RF voltage and the phase angle is shown in Fig. 6. The trapping efficiency is also strongly related to the initial kinetic energy because ions must penetrate the potential barrier to be transferred to the central part of the ion trap. Simulation of ions of 15 eV, 200 amu entering the ion trap when the RF phase is 0 ° (V_{RF} = + 750 $V_{0\text{-}p}$) show that the ion will be reflected back by the electric field in less than 0.2 μs. When the RF phase is 180 °, the ions will penetrate the ion trap and strike the electrode on the other side. This phenomena indicates that at an appropriate phase angle the ions can reverse their motion before reaching the entrance electrode. The relationship between trapping efficiency and initial RF phase for ions of different initial kinetic energy is shown in Fig. 7. Figure 7(a)–(c) correspond to the trapping efficiency of ions with initial kinetic energy of 25 eV, 15 eV and 5 eV respectively. The optimal phase range for 25 eV ions is 195 °–230 °. For the 15 eV ions the optimal phase range is 180 °–220 °. For the 5 eV ions the optimal range is 170 °–210 °. This important observation indicates that the initial RF phase angle, not the kinetic energy, is the determining factor of the trapping efficiency for ions with typical external injection energy. For ions which enter the ion trap outside the optimal phase range, for example, a 15 eV ion injected at 45 ° phase angle, the collision theory used here predicts that it will experience ~ 3–5 collisions as it travels through the ion trap. These collisions are not sufficient to remove the initial kinetic energy of the ions. Another observation (data not shown) is that ions which enter the ion trap at phase angles outside the optimal range will either be reflected by the electric field immediately or penetrate through the ion trap since an optimal energy range does not exist in which the ions will be trapped. The phase angle is calculated using ($2\pi\Omega t + \beta_0$), where Ω is the frequency of the AC voltage and β_0 is the initial phase angle (set to be 0 ° in current program). Since the optimal phase angle for external ion injection is around 200 °, the ions are first accelerated (the potential applied to the ring electrode is negative) when they enter the ion trap. The optimal phase angle ranges for 5 eV, 15 eV and 25 eV ions starts at 170 °, 180 ° and 195 ° respectively. This clearly indicates that ions of lower kinetic energy must be accelerated for a longer time to penetrate the energy barrier and reach the central region of the ion trap. If the initial acceleration process is too long ions will gain excess kinetic energy, traverse the ion trap and strike the exit end cap.

When the ions are generated in the pulsed mode (MALDI, for example), ideally the best trapping efficiency could be reached by allowing the ion to travel to the center of the ion trap and then turn on the RF potential very rapidly to the maximum amplitude (750 $V_{0\text{-}p}$ in our case). However, this scheme is difficult to implement in practice because of the difficulty of synchronizing RF turn-on with the ion injection event and the requirement to increase the RF potential in a very short time. Dynamic trapping is an alternative to the above method and is theoretically a better choice than the normal trapping method since it is not sensitive to the initial RF phase. The RF potential is gradually ramped up as ions enter the ion trap. Two important factors, RF ramp-up time and ion initial kinetic energy, determine the trapping efficiency when the ion m/z, V_d and V_{RF} are determined. The relationship between the trapping efficiency and ion initial kinetic energy is shown in Fig. 8(a). The molecular

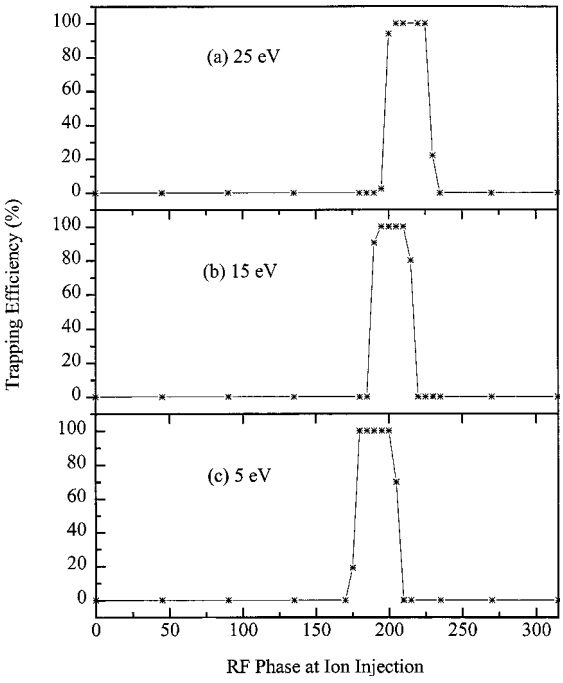

Figure 7. Trapping efficiency vs. RF phase in the normal trapping mode. The initial kinetic energy of the ions is (a) 25 eV, (b) 15 eV and (c) 5 eV for ions of 200 amu. V_{RF} = 750 $V_{0\text{-}p}$.

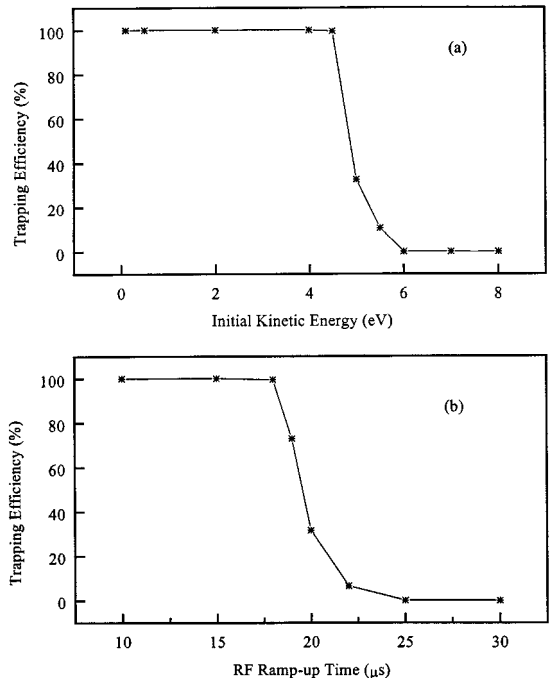

Figure 8. (a) Trapping efficiency vs. ion initial kinetic energy in the dynamic trapping mode, RF ramp-up time is 20 μs, V_d = 950 $V_{0\text{-}p}$, V_{RF} = 750 $V_{0\text{-}p}$, RF drop time is 10 μs, (b) trapping efficiency vs. RF ramp-up time in the dynamic trapping mode, V_d = 950 $V_{0\text{-}p}$, V_{RF} = 750 $V_{0\text{-}p}$ RF drop time is 10 μs. MW of the ion is 200 amu. The initial kinetic energy is 5 eV.

weight of each ion is 200 amu. The RF ramp-up time is 200 μs and the RF potential is ramped to 950 $V_{0\text{-}p}$. The RF potential then drop to 750 $V_{0\text{-}p}$ in 10 μs. According to these calculations, for a 5 eV ion 5 ~ 7 collisions occur between the ion and buffer gas molecules as it traverses the ion trap and before it strikes the exit electrode. About 30% of the ions are trapped when the initial kinetic energy is 5 eV at a pressure of 4 mTorr. When the ions enter the ion trap with kinetic energy greater than 6 eV, the current RF ramp-up rate is not sufficiently fast for the potential well to be deep enough to confine the ions inside the ion trap. To test the effect of the RF ramp-up rate on the trapping efficiency, the ramp-up time was changed and the trapping efficiency for ions of 5 eV initial kinetic energy was determined. The molecular weight of the ions is 200 amu in these studies. The result is shown in Fig. 8(b). When the ramp-up time is reduced, the trapping efficiency is increased accordingly. According to the data shown in Fig. 8(a) and (b), to improve the trapping efficiency in the external ion injection experiment, it is necessary to either increase the RF ramp-up rate or reduce the initial kinetic energy of the ions. When the sample probe is placed at the entrance end cap,[18] the ions generated will enter the ion trap in a narrow time window so that a fast ramping rate is critical for improving trapping efficiency. For ions generated outside the ion trap which are accelerated toward the entrance end cap, the ions will reach the end cap at different times. A practical approach is to have the ions reach the end cap when the RF is just partially ramped up[19–21,26] and the RF is rapidly ramped up to its maximum after the all ions have entered the ion trap. The ions will encounter a lower energy barrier when they enter the ion trap and will be trapped more easily compared to the standard trapping mode.

Resolution and extraction process

One of the major advantages of the ion trap/reflectron time-of-flight mass spectrometer is that the ion trap can accumulate ions to achieve a high duty cycle while also reducing the space and energy distributions through collisional cooling. The time distribution is negligible because all the ions are extracted simultaneously. SIMION uses a finite difference method, i.e. the over-relaxation method[24] to calculate the electric field in the space between the electrodes where the trajectory of an ion is calculated using a numerical integration method. The result is that simulation of ion movement over the entire IT/reTOF will generate a relatively large error for time-of-flight because of the error accumulation in integration and since only limited points are available to describe the region where the potential gradient is large. Instead, the time (t) for the ion to travel from the center of the ion trap to the detector can be described using the following function

$$t = t_1 + t_2 \tag{3}$$

where t_1 is the time interval from the start of the extraction pulse to the time when the ions cross Grid 1 in Fig. 1, and t_2 is the time for the ions to traverse from Grid 1 to the detector. After the physical dimensions of the IT/reTOF system are determined, t_2 becomes a function of an ion's m/z, kinetic energy at Grid 1 and the voltages applied to the reflectron grids. For a two stage reflectron system, the optimal voltage for the reflectron can be obtained by solving the following 2 differential equations:

$$\frac{\mathrm{d}}{\mathrm{d}V} t_2 = 0 \tag{4}$$

$$\frac{\mathrm{d}^2}{\mathrm{d}V^2} t_2 = 0 \tag{5}$$

where v is the velocity of the ion. Equations (4) and (5) can be numerically solved in Mathcad 6.0 and the optimal voltages for reflectron grids can be obtained. We calculated t_2 assuming that the initial positions for all ions with different initial kinetic energy are at Grid 1 in Fig. 1. The result is shown in Fig. 9 where in a broad kinetic energy range ($\pm$100 eV relative to the mean kinetic energy) the $t_2(KE)$-$t_2(KE_0)$ is within 2 ns for ions of 200 amu, where KE_0 is the mean kinetic energy and KE is the kinetic energy of each ion. This result indicates that if we could extract ions from the ion trap and achieve a space focusing at Grid 1, then the resolution could be optimized provided that the energy distribution at Grid 1 is within the optimal range. It is the distribution of the time at which ions cross Grid 1 which determines the resolution.

The electric field in the acceleration region is not linear because of the shape of the electrodes, it is thus difficult to use a mathematical equation to calculate the value of t_1. Instead, we use the SIMION program to

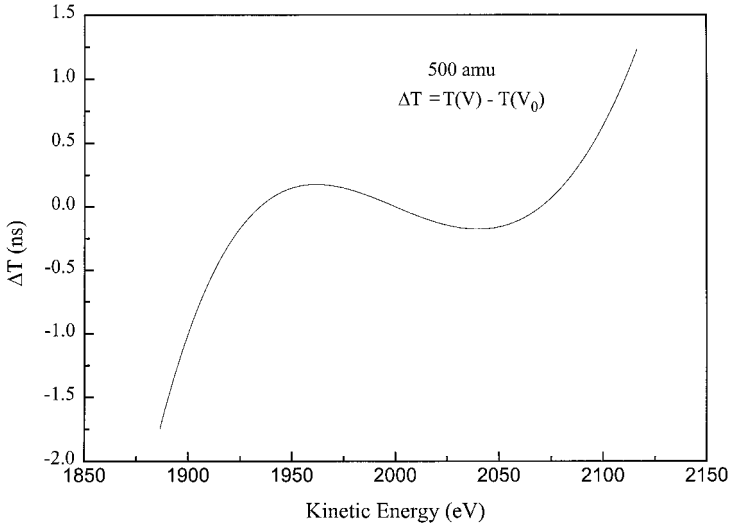

Figure 9. Δt_2 vs. initial kinetic energy of ion assuming the ions start at the same axial position (Grid 1). MW of the ion is 200 amu, liner voltage of the reTOF is –2000 V.

simulate the extraction process. First we create 50 random ions, trapped for 30 μs, then apply the extraction pulse(s). The time at which the ions cross Grid1 is recorded and a statistical analysis is performed.

We first investigate the energy distribution at Grid 1. +/–325 volts are applied to the entrance/exit end caps to eject the ions of 200 amu from the ion trap. The potential at the center of the ion trap is 0 V (RF potential on the ring electrode is 0 V in the extraction process). The potential at Grid 1 is –2000 V so the mean kinetic energy at Grid 1 should be 2000 eV. The calculated energy distribution is shown in Fig. 10. The mean of the kinetic energy is 1999.886 eV and this

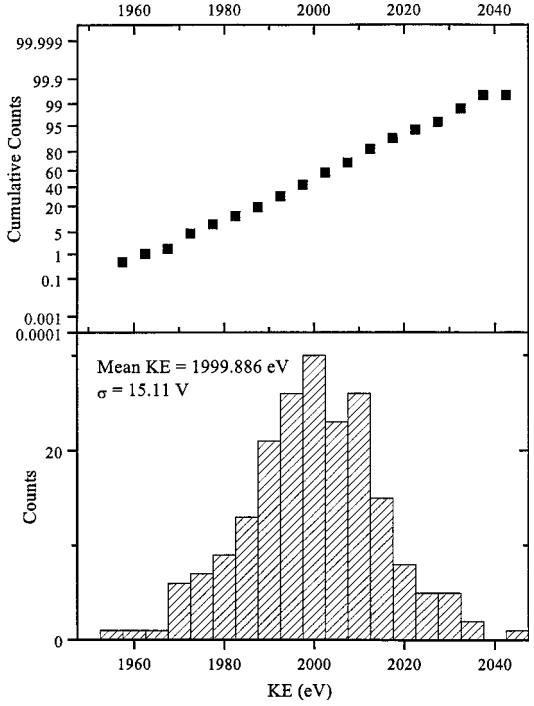

Figure 10. The energy distribution at Grid 1. Acceleration voltages are +/– 325 volts at entrance/exit end caps and the potential at Grid 1 is –2000 V. MW of the ion is 200 amu.

indicates that the accuracy of the simulation is very high. The standard deviation of the kinetic energy at Grid 1 is 15.11 eV and the energy range is from 1950 eV to 2040 eV, which is within the optimal range as shown in Fig. 9.

There are two schemes to apply the extraction pulse(s): (a) single pulsing, where either a negative pulse is applied to the exit end cap or a positive pulse is applied to the entrance end cap to eject the ions out from the ion trap; (b) bipolar pulsing, where a positive pulse and a negative (for example +/–325 V in the above example) are simultaneously applied to the entrance/exit end caps. Figure 11(a) is the contour of the electric field in the extraction region in the single pulsing mode and Fig. 11(b) is the contour of the electric field in the bipolar pulsing mode. The curves are quasi-potential lines. The distribution of the time (t_1) at which the ions cross Grid 1 after the extraction pulse(s) is (are) applied in both modes are shown in Fig. 12(a) and (b). It can be seen that the double pulsing scheme results in a much smaller time distribution. In the single pulsing mode, the electrical field at the center of the trap is strongly non-linear. Assuming the ions distribute symmetrically at the center of the ion trap, the ions whose starting position are closer to the entrance end cap will not be accelerated to sufficient velocity to achieve a space focusing at Grid 1. In the bipolar pulsing mode, the positive and negative pulses applied to the end caps create an electric field similar to a linear field. The force applied to the ions by the positive pulse on the entrance end cap makes it possible to spatially focus the ions at Grid 1.

In addition to the pulsing mode, the voltage of the pulses is another factor which determines resolution. The relation between the extraction voltage (absolute value) and the standard deviation of t_1 in the bipolar pulsing mode is shown in Fig. 13(a) for ions of 200 amu and Fig. 13(b) for ions of 500 amu. It can be seen that the best space focusing is achieved when the extraction voltage is 1100 V for ions of 200 amu and 1300 V for ions of 500 amu. The shift of the optimal extraction voltage indicates that the position of the focusing plane of the ions is also determined by m/z. Currently the

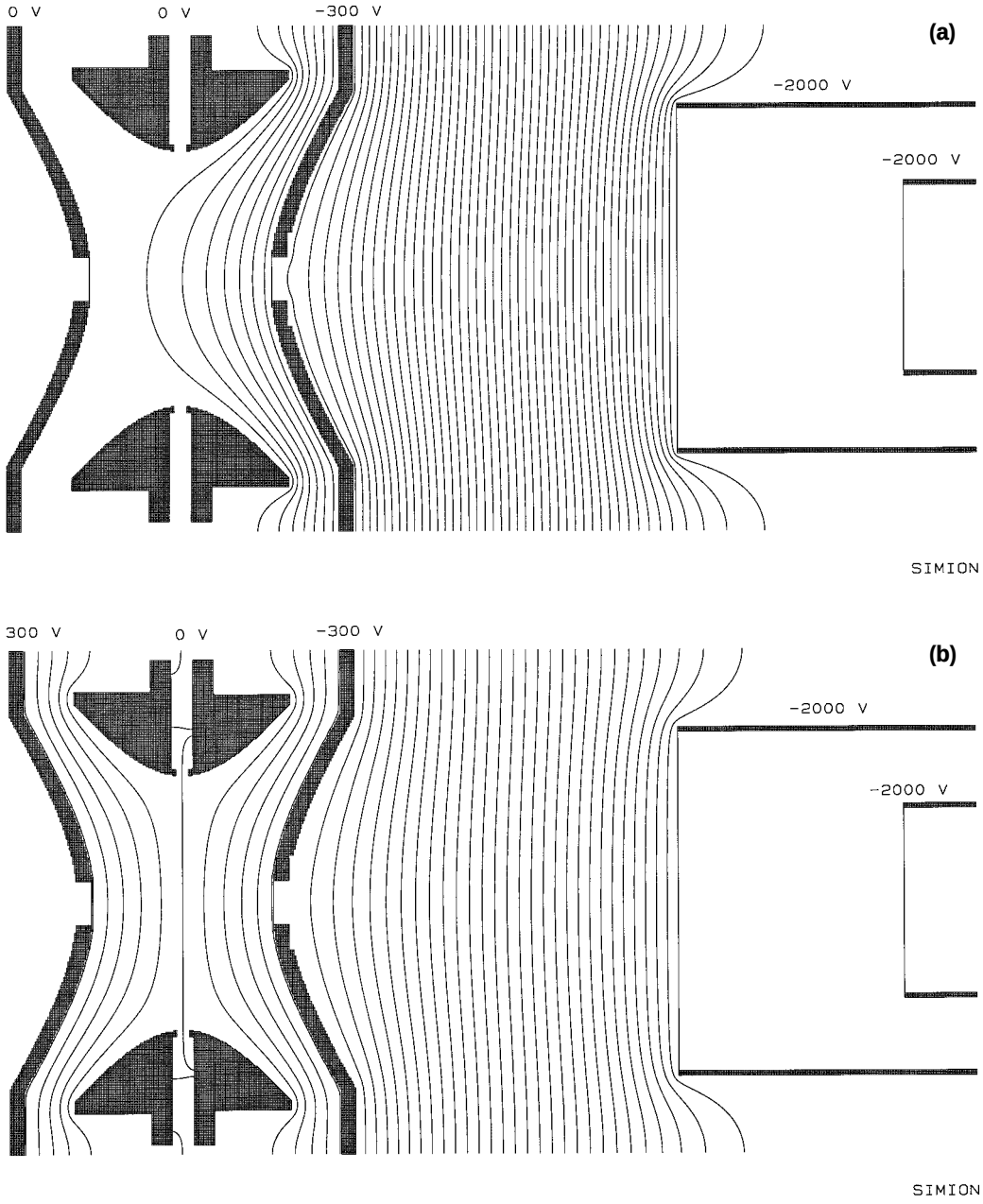

Figure 11. (a) The contour of the electric field inside the ion trap in the single pulsing mode, the entrance end cap is grounded and –300 V is applied to exit end cap. (b) The contour of the electric field inside the ion trap in the bipolar pulsing mode, +/–300 V are applied to the entrance/exit end caps.

liner voltage is –2000 V. If the liner voltage is doubled, the extraction voltage should also be increased. Theoretically higher extraction voltage and liner voltage can improve the resolution since the ions can be more tightly compacted spatially.

The ions could be extracted from the ion trap under two conditions: (a) RF voltage is on; (b) RF voltage is off. The relation between the mass resolution and the RF phase at extraction has been reported by other groups.[9,27] It has been found that applying the extraction pulse when the ring electrode voltage is most negative results in the best resolution. However, in the process in which the ions are extracted from the ion trap, the oscillating electric field created by the ring electrode will impose different effects on the ion kinetic energy depending on the dimension of the ion trap, m/z of the ions, and the extraction voltage. An alternative approach is to apply the extraction voltage after the RF voltage is shut down to 0 V very rapidly (tens of nanoseconds to several microseconds). It is expected that the RF ramp-off rate is related to the resolution. A slower ramp-off rate may cause the ions to expand and the initial space distribution is enlarged. According to the phase space dynamics methods,[28] the distribution of ion position and velocity is related to the RF phase. A rapid ramp-off is better for preventing ion spatial expansion, but the RF phase at which the ramp-off starts will influence the extraction process. We have simulated the relation between space focusing at Grid 1 and ramp-off rate and the result is shown in Fig. 14. Two hundred ions of 200 amu are used in this simulation. The RF ramp-off starts when the RF is at its maximum

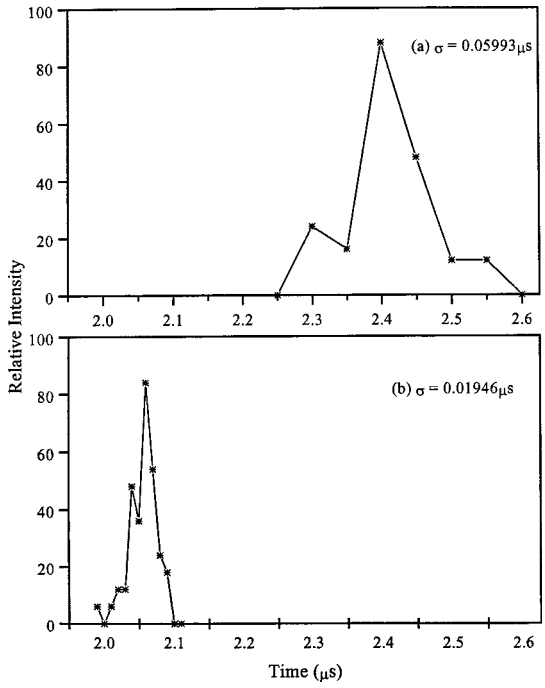

Figure 12. (a) The distribution of the time at which ions cross Grid 1 in the single pulsing mode, (b) the distribution of the time at which ions cross Grid 1 in the bipolar pulsing mode. +/–325 volts are applied to the entrance/exit end caps, MW of the ion is 200 amu. Liner voltage is –2000 V.

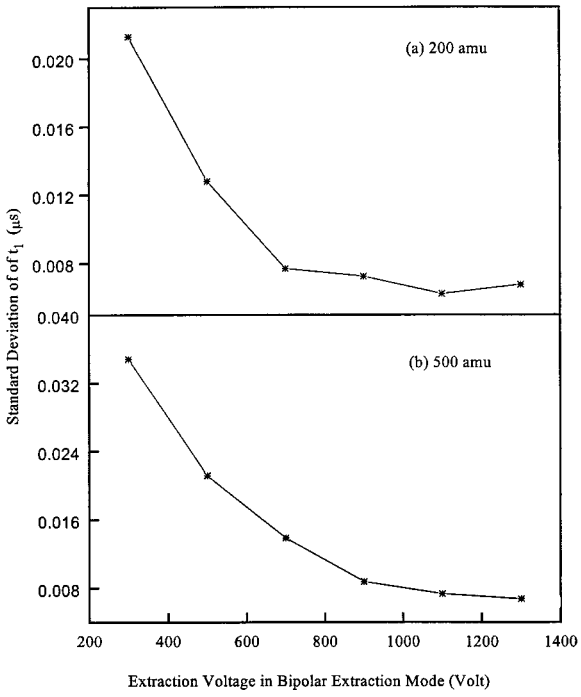

Figure 13. The standard deviation of the time at which ions cross acceleration Grid 1 vs. the extraction voltage in the bipolar pulsing mode for ions of (a) 200 amu, (b) 500 amu. Liner voltage is –2000 V.

positive voltage. From the chart we can see that when the shut-down time is about 1 μs the variation in t_1 is minimal.

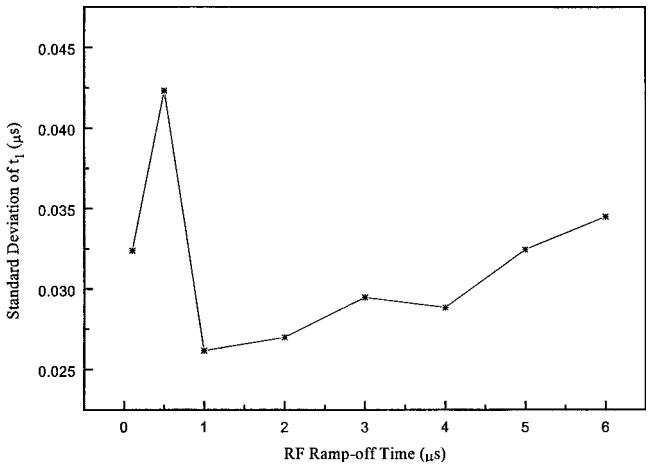

Figure 14. The standard deviation of the time at which ions cross Grid 1 vs. the RF shut down time. +/–325 V are applied to the entrance/exit end caps. Liner voltage is –2000 V.

CONCLUSION

We have used the SIMION 6.0 program to simulate the ion motion inside the ion trap and to generate statistical results regarding trapping efficiency and resolution. A 3D orthogonal collision model has been implemented in the user program to simulate the effects of buffer gas. The MathCad 6.0 program has been used to generate initial positions of ions using a Gaussian distribution and to numerically solve the differential flight time equations for a reTOF system to obtain optimal reflectron voltages. It has been observed that there is a phase-shift of the optimal range for external ion injection and this shift is related to the ion initial kinetic energy. The trapping efficiency in the dynamic trapping mode is determined by the initial kinetic energy and the RF ramp-up rate. A fast ramp-up rate for the RF potential is necessary to improve the trapping efficiency for ions with higher initial kinetic energy. The resolution of the IT/reTOF mass spectrometer is determined by the extraction process. Bipolar pulsing provides a push–pull force to eject the ions from the ion trap and results in an improved scheme for spatially focusing the ions at the acceleration grid (Grid 1 in Fig. 1) compared to the single pulsing method. The m/z of the ions and the voltages applied to the entrance/exit end caps determine the actual position of the focusing plane.

Acknowledgement

We gratefully acknowledge support of various aspects of this work by the National Institutes of Health under Grant No. 1R01GM49500 and the National Center for Human Genome Research under Grant No. 1R01HG0068503 and the National Science Foundation under Grant No. BIR-9513878.

REFERENCES

1. G. C. Stafford, P. E. Kelley, J. E. P. Syka, W. E. Reynolds and J. F. Todd, *Int. J. Mass Spectrom. Ion Processes* **60**, 85 (1984).
2. B. M. Chien, S. M. Michael and D. M. Lubman, *Rev. Sci. Instrum.* **63**, 4277 (1992).
3. J. T. Wu, P. Huang, M. X. Li and D. M. Lubman, *Anal. Chem.* **69**, 2908–2913 (1997).
4. M. X. Li, L. Liu, J. T. Wu and D. M. Lubman, *Anal. Chem.* **69**, 2451 (1997).
5. M. G. Qian and D. M. Lubman, *Rapid Commun. Mass Spectrom.* **10**, 1991 (1996).

6. M. G. Qian, Y. Zhang and D. M. Lubman, *Rapid Commun. Mass Spectrom.* **9**, 1275 (1995).
7. M. G. Qian and David M. Lubman, *Anal. Chem.* **67**, 234A (1995).
8. H. Lee and D. M. Lubman, *Anal. Chem.* **67**, 1400 (1995).
9. P. Kofel, M. Stöckli, J. Krause and U. P. Schlunegger, *Rapid Commun. Mass Spectrom.* **10**, 658 (1996).
10. R. E. March, A. W. McMahon, F. A. Londry, R. L. Alfred, J. F. J. Todd and F. Vedel, *Int. J. Mass Spectrom. Ion Processes* **95**, 119 (1989).
11. R. E. March, A. W. McMahon, E. T. Allison, F. A. Londry, R. L. Alfred, J. F. J. Todd and F. Vedel, *Int. J. Mass Spectrom. Ion Processes* **99**, 109 (1990).
12. R. E. March, F. A. Londry, R. L. Alfred, J. F. J. Todd, A. D. Penman, F. Vedel and M. Vedel, *Int. J. Mass Spectrom. Ion Processes* **110**, 159 (1991).
13. C. Ma, H. Lee and D. M. Lubman, *Appl. Spectrosc.* **46**, 1769 (1992).
14. R. K. Julian, M. Nappi, C. Weil and R. G. Cooks, *J. Am. Soc. Mass. Spectrom.* **6**, 57 (1995).
15. C. Weil, M. Nappi, C. D. Cleven, H. Wollnik and R. G. Cooks, *J. Am. Soc. Mass. Spectrom.* **10**, 742 (1996).
16. M. N. Kishore and P. K. Ghosh, *Int. J. Mass Spectrom. Ion Phys.* **29**, 345 (1979).
17. J. F. J. Todd, D. A. Freer and R. M. Waldren, *Int. J. Mass Spectrom. Ion Phys.* **36**, 371 (1980).
18. V. M. Doroshenko and R. J. Cooks, *Rapid Commun. Mass Spectrom.* **7**, 822 (1993).
19. J. Qin and B. T. Chait, *Anal. Chem.* **68**, 1784 (1996).
20. J. Qin and B. T. Chait, *Anal. Chem.* **68**, 2108 (1996).
21. J. Qin and B. T. Chait, *Anal. Chem.* **68**, 2102 (1996).
22. C.-S. O. and H. A. Schuessler, *J. Appl. Phys.* **52**, 1157 (1981).
23. R. D. Knight, *Int. J. Mass Spectrom. Ion Phys.* **51**, 127 (1983).
24. David A. Dahl, *Simion 3D Version 6.0 User's Manual* (1995).
25. E. Fischer, *Z. Phys.* **156**(1), 1 (1959).
26. L. He, Y. Liu, Y. Zhu and D. M. Lubman, *Rapid Commun. Mass Spectrom.* **11**, 1440 (1997).
27. U. Wilhelm, C. Weickhardt and J. Grotemeyer, *Rapid Commun. Mass Spectrom.***10**, 473 (1996).
28. R. E. March, in *Quadrupole Storage Mass Spectrometry*, Wiley, New York (1989).